International Forum on Aeroelasticity and Structural Dynamics
IFASD 2017
25-28 June 2017, Como - Italy

AEROELASTIC ANALYSIS OF DOUBLE-SWEPT ROTOR BLADE IN HOVERING CONDITIONS

M. Rohin Kumar[1], and Lokeswara Rao. V[2]

[1]Institute of Flight Systems, Rotorcraft
DLR, Braunschweig, Germany
rohin.majeti@dlr.de

[2] Manager, PhD candidate
Rotary Wing Research and Design Centre,
Hindustan Aeronautics Limited, India
dyna.rwrdc@hal-india.com

Keywords: Double-sweep, rotary-wing aeroelasticity, structural dynamics.

Abstract: The double-sweep is a relatively new advanced blade shape employed in the rotorcraft industry, mainly, to alleviate rotor noise. The aeroelastic effects of this advanced shape have been relatively less discussed in the open literature. The current work involves a study concerning the effects of a double-sweep, along with a tip-anhedral, on the aeroelastic loads and structural dynamics of a rotor blade. For carrying out this analysis, a comprehensive simulation tool employing the Peters-He dynamic wake model and the ONERA dynamic stall model for air loads is used. It is shown that the double-sweep geometry causes large lag shear forces, lag as well as torsional moments at the blade root and at the double-sweep junction.

NOTATION

ONERA	Office National d'Etudes et Recherches Aérospatiales (French Aerospace Lab)
DLR	Deutsches Zentrum für Luft- und Raumfahrte.V. (German Aerospace Center)
BVI	Blade Vortex Interaction
ERATO	Etude d´un Rotor Aéroacoustique Technologiquement Optimisé (Aeroacoustically optimized rotor)

1 INTRODUCTION

Advanced blade shapes have been used in helicopter rotors for performance enhancement and noise alleviation. One such technology is the Blue Edge^{TM} concept [1, 2] developed by Airbus Helicopters in association with ONERA. The Blue Edge^{TM} blade, featuring double-sweep and tip-anhedral, is a passive BVI-noise reduction concept based on the ERATO project [3, 4] which was carried out within the framework of cooperation between ONERA, DLR and Airbus Helicopters. Apart from this fact, not much information has been published in open literature with regards to the precise geometric details of the blade. While it has been claimed that the advanced shape of the blade reduces helicopter noise by 3-4 dB, its effects on structural dynamics and vibratory loads have not been discussed much in literature. In [2], for example, the presence of high loads at the double-sweep junction (intersection between forward and backward sweeps) of the ERATO blade and the need for torsional stiffening of the blade is indicated without going into any specific details. Similarly, in [4], aeroelastic tailoring of the Blue Edge^{TM} blade is discussed with little quantitative details.

The objective of the current work is to study the effects of giving a double-sweep along with a tip-anhedral (similar to the Blue Edge^{TM} shape) to a rotor blade of known geometric properties. No structural or aerodynamic optimization studies were done for the shape of the blade. This is a preliminary study carried out to understand the kind of aeroelastic loads generated by introduction of a pre-determined double-sweep in an isolated rotor. It is to be noted that for the purpose of this paper, the term double-sweep includes the tip-anhedral as well. The tip-anhedral is retained for its potential benefits from aerodynamic and acoustic considerations which shall be the topic for a future study. In addition, the effects of the double-sweep shape on the aeroelastic stability of the rotor blades will be determined in future studies.

The prediction of loads and response of the helicopter rotor requires a comprehensive analysis program. Since helicopter rotor loads and response evaluation is an aeroelastic problem, the comprehensive analysis tool comprises of structural, inertia as well as aerodynamic models. The comprehensive analysis program used for the current study has been described in detail and validated in [5]. Using this program, the effects of tip-sweep and tip-anhedral on the structural dynamics and trim characteristics were studied in [6-7]. As is well known, it was found that sweep in a rotor blade introduces bending-torsion coupling while anhedral/dihedral introduces bending-axial coupling. The studies [6-7] concluded that in hovering conditions, both tip-sweep and tip-anhedral reduce the nose-down elastic torsion deformation in the rotor blade. It was also concluded that both tip-sweep and tip-anhedral reduce the 1Ω harmonics of the blade root loads while increasing the 4Ω harmonics of the hub loads in a 4-bladed rotor.

2 ANALYSIS

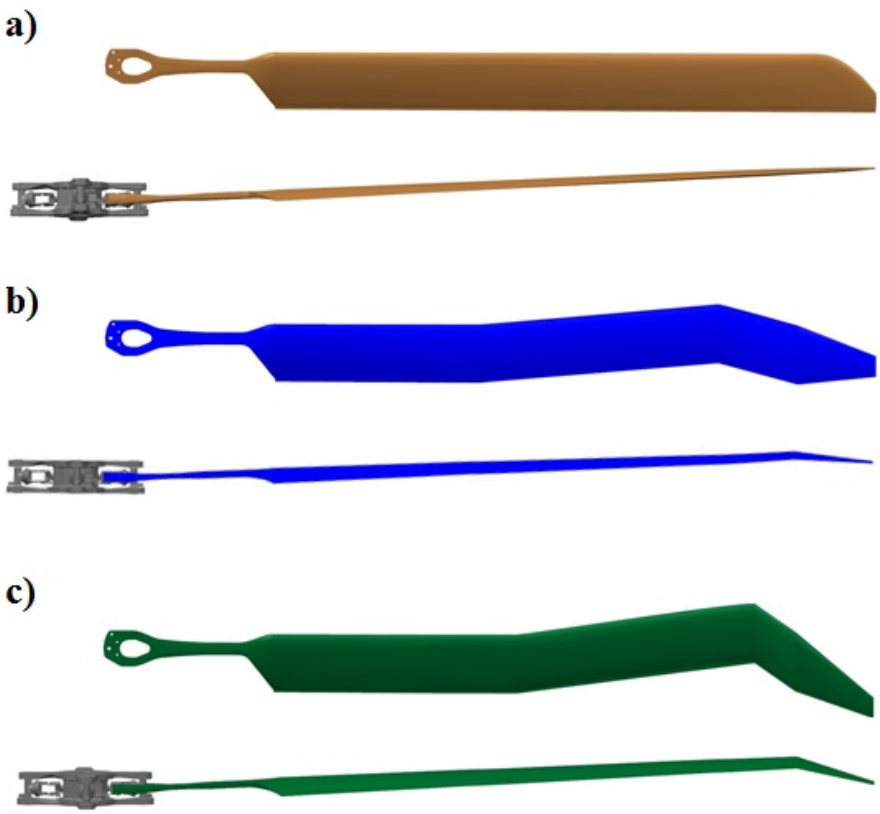

Figure 1: Blade geometry of the three blades used for analysis

For the current analysis, the behavior of a baseline unswept blade was compared with those of two blades given the double-sweep shape along with a tip-anhedral. A straight, twisted blade is taken as the baseline blade – 'blade *a*' - whose structural properties are based on a real blade. Two generic blades ('blade *b*' and 'blade *c*') with the same cross-sectional inertia and stiffness properties as the baseline blade were given the double-sweep shape and a tip-anhedral angle (Fig. 1). The sweep and anhedral angles information of the three blades is given in Table 1. The elastic axis, center of gravity and the aerodynamic center are assumed to be coincident at every section. While deciding the lengths of the swept part of the blade, rotor loading in free-flight hover was taken into consideration. The lengths of the forward-swept part and the backward-swept part of the blade were chosen so as to keep the torsional moment about the original straight-line feathering axis to a minimum. The baseline blade has constant chord 'c' with a parabolic tip. The non-dimensional chord (c/R) was taken as 0.0757, where 'R' is the length of the blade. The airfoil section begins at 0.25 R. The rotor blade is assumed to have the same airfoil throughout its length. The blade has a pretwist of -12^o from the root to the tip with geometric twist at the tip equal to 4^o. The reference blade mass distribution (m_o) was taken as 8.45 kg/m. The rotor radius 'R' was kept the same for all the three blades and is 6.6 m. The non-dimensional inertia and stiffness distribution curves for blade *a* are given in Fig. 2 and Fig. 3. The non-dimensional factor used for inertia is m_oR^2 and for stiffness, it is $m_o\Omega_oR^4$.

		Forward sweep	Backward sweep	Tip anhedral
Blade *a*	Angle	0	0	0
	Region	-	-	-
Blade *b*	Angle	5^o	15^o	5^o
	Region	0.5R-0.8R	0.8R-1.0R	0.9R-1.0R
Blade *c*	Angle	7.5^o	35^o	15^o
	Region	0.55R-0.85R	0.85R-1.0R	0.9R-1.0R

Table 1: Blade sweep and anhedral details

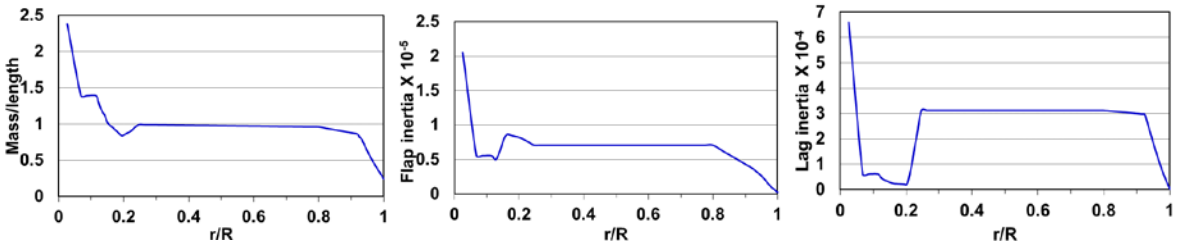

Figure 2: Property distribution (non-dimensional) along the baseline blade length for mass, flap inertia, and lag inertia

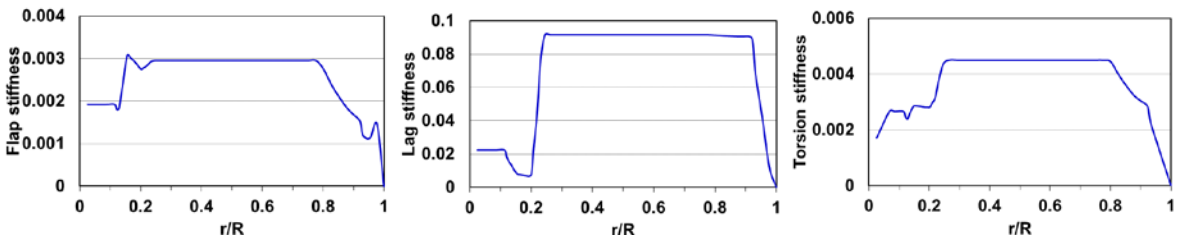

Figure 3: Stiffness distribution (non-dimensional) along the baseline blade length in the direction of flap, lag, and torsion

For finding the structural dynamics characteristics, the rotor blade was modelled using finite elements, with each element having 14 degrees of freedom. The rotor blade is modelled using rotating, long, slender beam-type finite elements. Equations of motion of the blade were derived using Hamilton's principle. The strain-displacement relationships were considered as moderate, with couplings in flap, lag, torsional and axial deformations. Formulations for rotor blade includes geometry features like pre-cone, pre-sweep, pre-droop, pre-twist, torque offset, hinge offset, swept and anhedral tips. The linear, undamped model is solved in the finite element domain to obtain the natural frequencies and the corresponding mode shapes of the rotating blade. The governing equation for the i^{th} finite blade element is

$$[M_i]\{\ddot{q}_i\} + [K_i]\{q_i\} = 0 \tag{1}$$

where $[M_i]$ represents the mass matrix of the i^{th} element and $[K_i]$ the stiffness matrix.

For rotor blades with a sweep and/or anhedral, the governing equation for the corresponding blade element is given by

$$[\Lambda]^T[M_t][\Lambda]\{\ddot{q}_t\} + [\Lambda]^T[K_t][\Lambda]\{q_t\} = 0 \tag{2}$$

where $[\Lambda]$ is the local-to-global transformation matrix for blade elements with sweep and anhedral [6].

The global aeroelastic equation for the whole blade is obtained by assembling the elemental matrices from the kinetic and strain energy contributions,

$$[M]\{\ddot{q}\} + [C]\{\dot{q}\} + [K]\{q\} = \{F_{AD}\} \tag{3}$$

where $[C]$ is the damping matrix and $\{F_{AD}\}$ is the aerodynamic force contribution.

The derivation and validation of the structural and aerodynamic models and the procedures for complete aeroelastic analysis have been explained in detail in [5, 6]. To reduce the total number of degrees of freedom, the rotor blade aeroelastic loads problem is transformed from the finite-element domain to the modal domain by modal transformation. Eight modes comprising flap, lag, torsion and axial modes were used in the modal transformation. The rotor aerodynamics module has several hierarchical models, of which the generalized dynamic wake theory (Peters-He) [8] for inflow and ONERA dynamic stall theory [9, 10] for airloads calculations are the most prominent ones.

The Peters-He [8] dynamic wake model is a compact, closed-form formulation with multiple states that allow variation of the inflow in the radial as well as azimuthal directions. The inflow is represented as an infinite series in radial and harmonic functions. The inflow states are evaluated by solving a set of differential equations. In this model, the total inflow is a function of azimuth, time, and radial station. It was concluded in [11] that for a 4-bladed rotor, 15 inflow states (4 harmonics) in the dynamic wake theory sufficiently captured the inflow effects.

The ONERA model [9, 10] describes the unsteady airfoil behaviour in both attached flow and separated flow using a set of nonlinear differential equations. The lift, moment and drag of an oscillating airfoil are given in terms of attached flow circulation and detached flow 'circulation'. These circulations are determined as solutions to differential equations. The stall model assumes that the lift, moment and drag are acting at the quarter chord point.

The current work is concerned with only the whirl tower analysis (isolated rotor). In whirl tower tests, the rotor is mounted above the ground on a vertical stand with a motor with actuators to change rotor collective and cyclic pitch input. The flowchart in Fig. 4 summarizes the procedure for whirl tower analysis. The loads, inflow and response equations are all in the form of differential equations and solved iteratively till a converged solution is obtained over several revolutions for a given set of rotor control inputs. The blade equations and the aerodynamic equations are evaluated at alternate time steps for a whole revolution. The sectional aerodynamic loads are calculated at 15 prescribed equidistant stations on the rotor blades. The root loads are obtained by integration of the sectional loads over the length of the blade using Simpson's rule. The analysis was implemented as a C++ program using the open-source GSL [12] as the math library. The blade and aerodynamic differential equations were solved using the Runge-Kutta method. The simulation parameters and rotor data for the whirl tower analysis is given in Table 2.

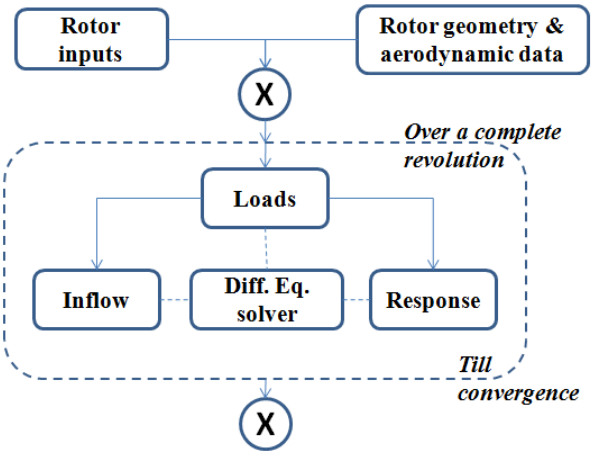

Figure 4: Flowchart for whirl tower (isolated rotor) analysis

Parameters		**Value**
Number of blades	N_b	4
Air density at sea level	ρ (kg/m^3)	1.224
Blade mass distribution	m_0 (kg/m)	8.45
Solidity ratio	σ	0.09646
Radius	R (m)	6.6
Weight coefficient	C_w	0.00734
Lift-curve slope	$C_{l\alpha}$	5.73
Profile drag coefficient	C_{d0}	0.01
Lock number	γ	6.4
Pre-twist	(deg)	-12
Pre-droop	β_d (deg)	2.5
Rotational speed	Ω (rad/s)	32.8

Table 2: Simulation parameters and rotor data

3 RESULTS

3.1 Structural Dynamics

The Campbell diagram of the three rotor blades at a rotational speed of 32.8 rad/s are given in Fig. 5 for comparison. The variations of the first 6 (I-VI) natural frequencies with rotational speed are shown. The corresponding modes have been identified only for the straight blade and not for the other two blades. This is because in the case of double-swept blades, the bending-torsion coupling due to sweep makes it difficult to categorize them as bending mode or torsion mode. In fact, the IV, V and VI frequencies have large torsional content in their modes for the double-swept blades, especially at higher rotational speeds. The strong bending-torsion coupling in the blades can lead to aeroelastic instability problems. Aeroelastic stability of the double-swept blades and appropriate structural modifications to avoid instabilities shall be taken up in a future study. The first axial mode has a high natural frequency on account of high axial stiffness and hence, could not be shown here.

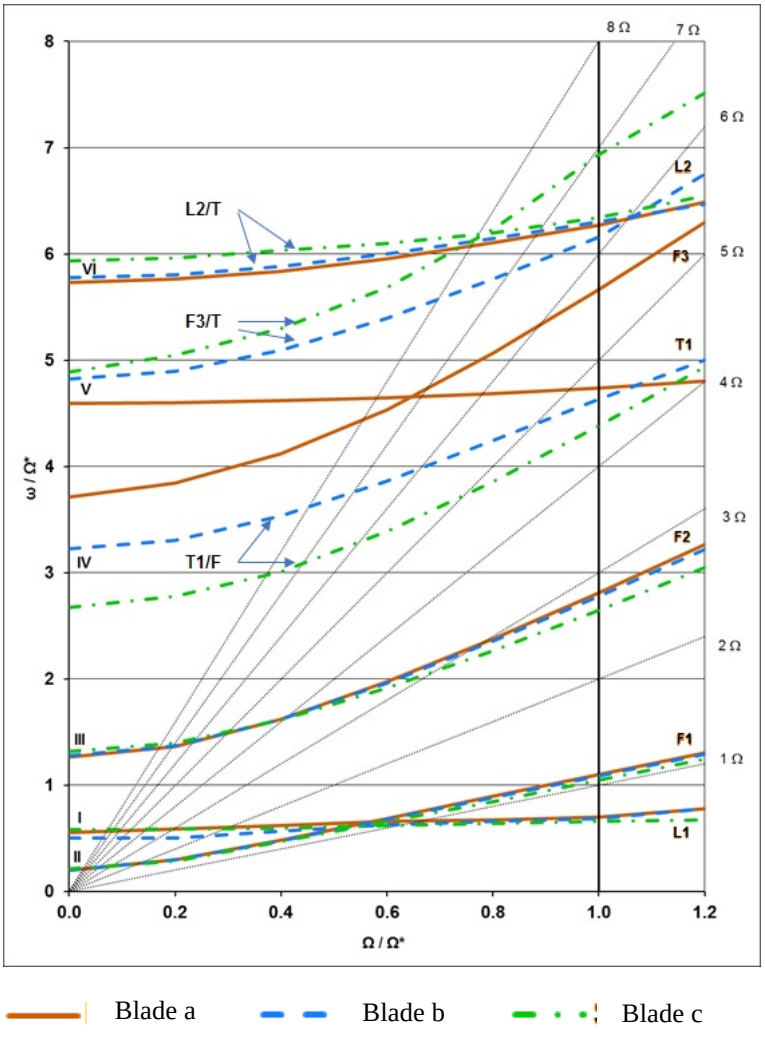

Figure 5: Campbell diagram for the three rotor blades under study (L-lag, F-flap, T-torsion)

In the case of rotor blades with sweep/anhedral, apart from the mass and stiffness distribution, additional factors affect the natural frequencies. The double-sweep of the blade results in forward offset of the center of gravity from the feathering axis of the rotor blade. In [6], it was shown that tip-sweep and tip-anhedral have only minor influence on the bending frequencies. It was also seen that tip-anhedral slightly reduces the fundamental torsional frequency.

As far as the blade natural frequencies are concerned, there is not much cause for concern with respect to resonance with rotor rotational speed due to the double-swept shapes. For hingeless rotors, in general, having lower flap frequencies than 1.1Ω results in reduced vibration and gust response ([13]). For the baseline blade *a* as well as for blades *b* and *c*, the fundamental natural frequencies are between 1.05Ω and 1.1Ω. Fundamental lag frequency has a desirable value between 0.6Ω and 0.8Ω for acceptable air and ground resonance instabilities and acceptable loads ([13]). The fundamental lag frequency (I) for the baseline blade is about 0.68Ω. It decreases slightly for blade *b* and blade *c* but since it is maintained above 0.65Ω, there is no cause for concern. The 2nd flap frequency (III) is shifted to lower frequencies which is desirable to avoid resonance with the third harmonic of the rotor rotational speed. The 1st torsion (IV) and the 3rd flap (V) frequencies are the most affected by the double-sweep. However, they are well clear of 3Ω, 4Ω, and 5Ω. The frequency of blade *c* corresponding to the 3rd flap frequency of the baseline blade is very close to 7Ω which is a cause for concern. Some stiffening measures in the flap direction would be required to increase the gap.

3.2 Whirl tower loads

The rotor is first given only collective angle inputs ranging from -9^o to 3^o which translates to -1.8^o to 10.2^o at 0.7R where the geometric twist is 7.2^o. In the next case, a combination of collective and cyclic angles is given as input.

In [6], it was seen that tip-anhedral has minor influence on the overall thrust, root shear force and bending moments. Also, the angle of the tip-anhedral being relatively small, its effects on the loads are largely overshadowed by effects of the larger sweep angles. The double-sweep geometry causes an offset of the sectional aerodynamic center and the center of gravity from the feathering axis. The aerodynamic lift, centrifugal and the inertia forces acting on the double-sweep part of the blade, thus, introduce pitching moments about the feathering axis. Apart from this, the aerodynamic drag forces on the forward-swept and the backward-swept parts of the blade partially cancel each other as they are inclined in opposite directions to the straight portion of the blade. Another major effect comes from the large centrifugal force on the double-swept part of the blade. Because of the offset of the center of gravity of this region, the large centrifugal force has components along all the three coordinate axes resulting in contributions to lag shear forces and moments as well as the torsional moment about the feathering axis. Thus, the net shear forces and bending/torsional moments are influenced by aerodynamic, inertia and centrifugal forces whose magnitudes are functions of parameters such as rotational speed, sweep angles, sweep lengths etc.

3.2.1 Collective input

Figure 6 shows the effects of the double-sweep feature on thrust and power coefficients. The coefficient factors used are $\rho A(\Omega R)^2$ for thrust, $\rho A(\Omega R)^3$ for power and $\rho A(\Omega R)^2 R$ for moments. With increase in the sweep and anhedral angles, there is only a slight change in the thrust and power curves. It is interesting that at 10.2^o collective which is approximately the collective angle in free-flight hover, blades *b* and *c* require slightly lesser power than blade *a* (Fig 7b).

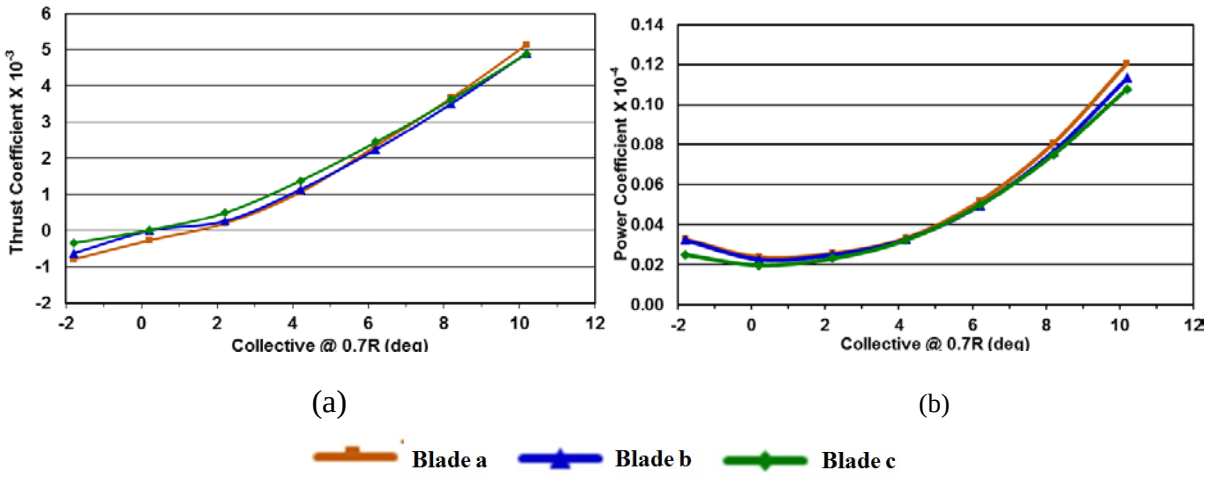

Figure 6: (a) Thrust and (b) power coefficient variation with variation in collective control

Figure 7 shows the flap and lag shear forces at the root for the three blades. The root flap shear forces of the 3 blades do not vary much (Fig 7a). This agrees with the thrust curves in Fig. 6 since the total thrust is a summation of the contributions from all the blades. However, there is a large increase in the root lag shear force for the blade *b* and blade *c* over blade *a* (Fig 7b).

Figure 8 shows the root moments for the three blades. The flap moments decrease with increase in sweep angles, especially at higher collective angles (Fig 8a). The root lag moments for blades *b* and *c* are lesser compared to blade *a* (Fig 8b). With regards to the root torsional moment (Fig 8c), while blade *a* is uniformly subjected to pitch-up moments, blade *b* and blade *c* are subjected to pitch-up moments at lower collective angles and high pitch-down moments at higher collective angles. The root torsional moment is an important design criteria as it is transferred to the pitch-link as axial force. The fact that blade *c* has lower root torsional moment than blade *b* suggests that it is possible to keep this load to a minimum by proper selection of the double-sweep shape.

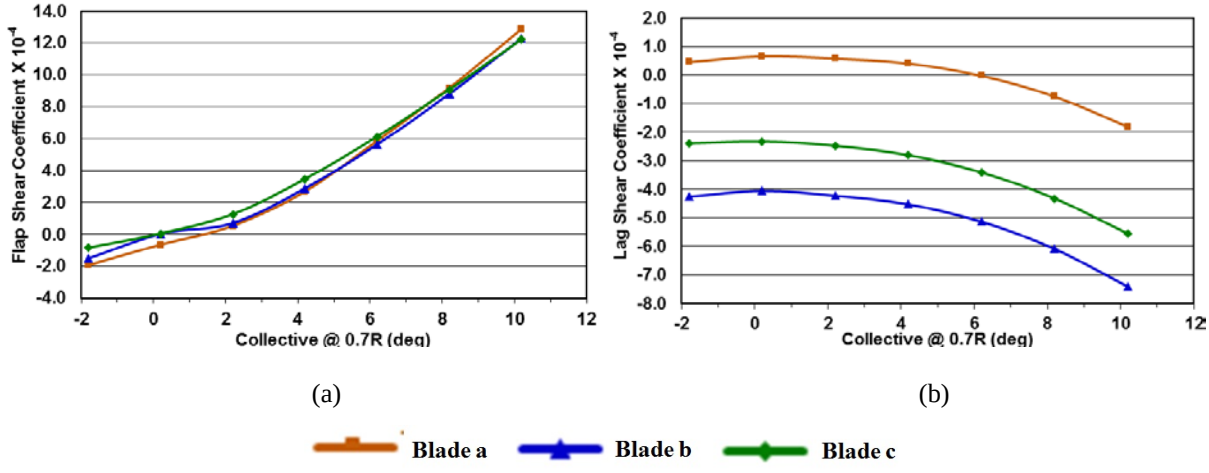

Figure 7: Root a) flap and b) lag shear force variation with variation in collective control

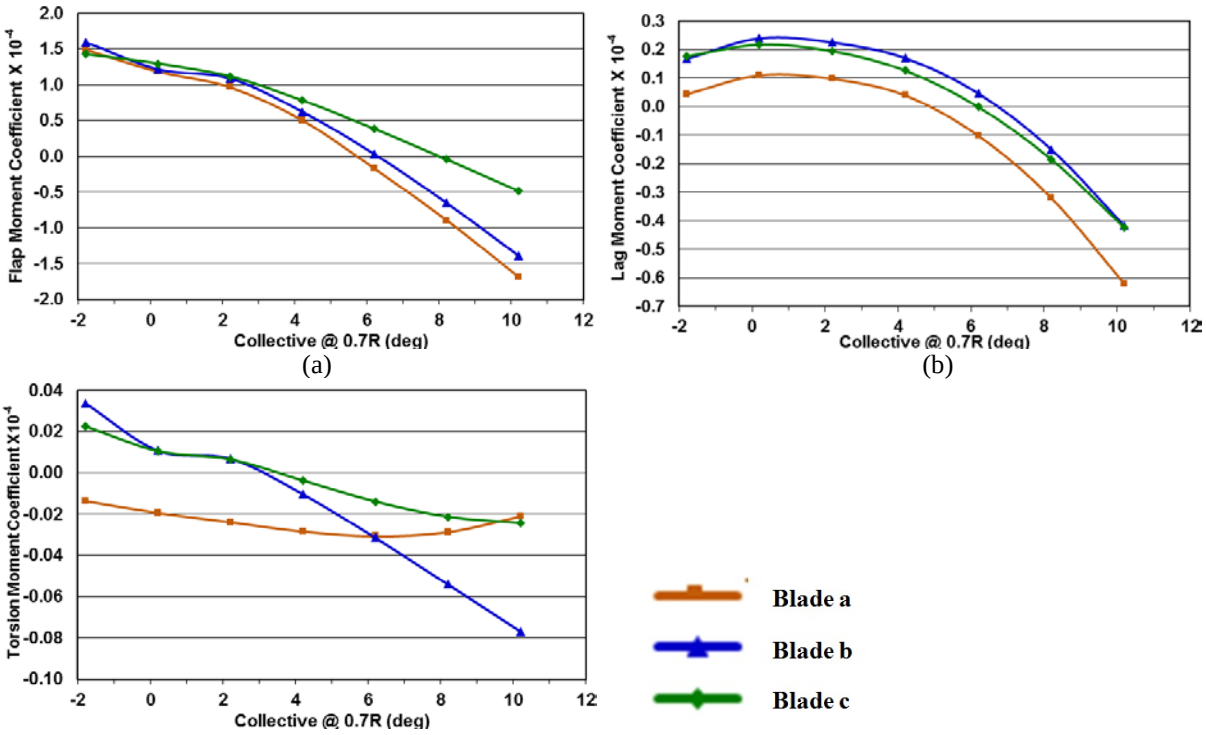

Figure 8: Root moments variation with variation in collective control

From the above exposition, it is seen that the double-sweep shape has some benefits in that it reduces the flap and lag bending moments at the root. The large lag shear force and root torsional moments are a matter of concern. However, by proper selection of the double-sweep shape parameters (angles), these loads can be minimized. Additional stiffening measures at the root may also be taken.

The junctions of geometry changes in the rotor blade are important sections from design considerations. Figure 9 shows the shear forces at the junction between the forward-swept and backward-swept portions of the blade and at 0.8R of the baseline blade. The flap shear forces of the blade *c* have slightly decreased as compared to those of the baseline blade (Fig 9a). The lag shear forces of blade *b* and blade *c* are larger than those of the baseline blade (Fig 9b). In the case of blade *c*, the lag shear force at the junction is subdued because of the large backward sweep angle leading to lesser drag in the direction perpendicular to the original feathering axis.

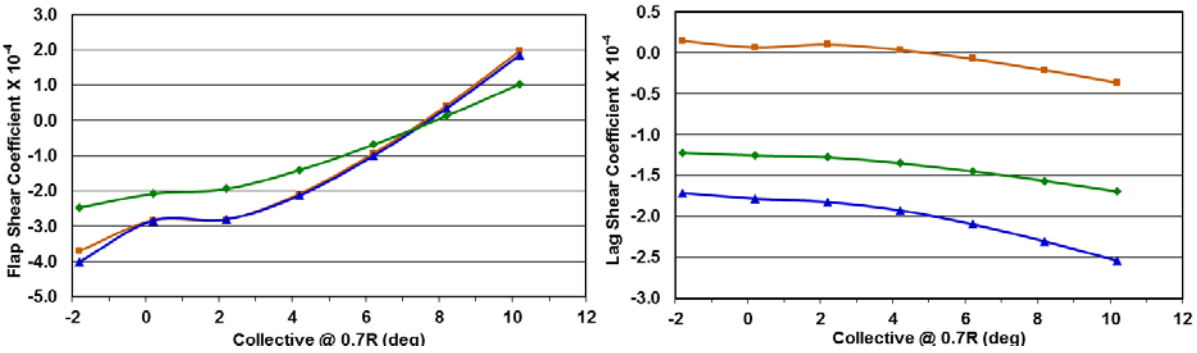

Figure 9: Double-sweep junction shear force variation with variation in collective control

Figure 10 gives the moments at the junction between the forward-swept and backward-swept portions of the blade and at 0.8R of the baseline blade. The flap moment of blade *b* at the sweep junction is lesser than that of the baseline blade while the flap moment of blade *c* is of opposite sign for higher collective angle (Fig 10a). Regarding lag moment at the sweep junction, the lag moments of blade *b* and blade *c* have increased tremendously over that of the baseline blade (Fig 10b). The torsional moment at the sweep junction blade *b* and blade *c* are larger than those for blade *a* for lower collective angles but for higher angles, they are comparable (Fig 10c).

The above analysis indicates the need to sufficiently stiffen the sweep junction to take into consideration any increase in stresses due to increase in lag shear forces and lag moments at the junction.

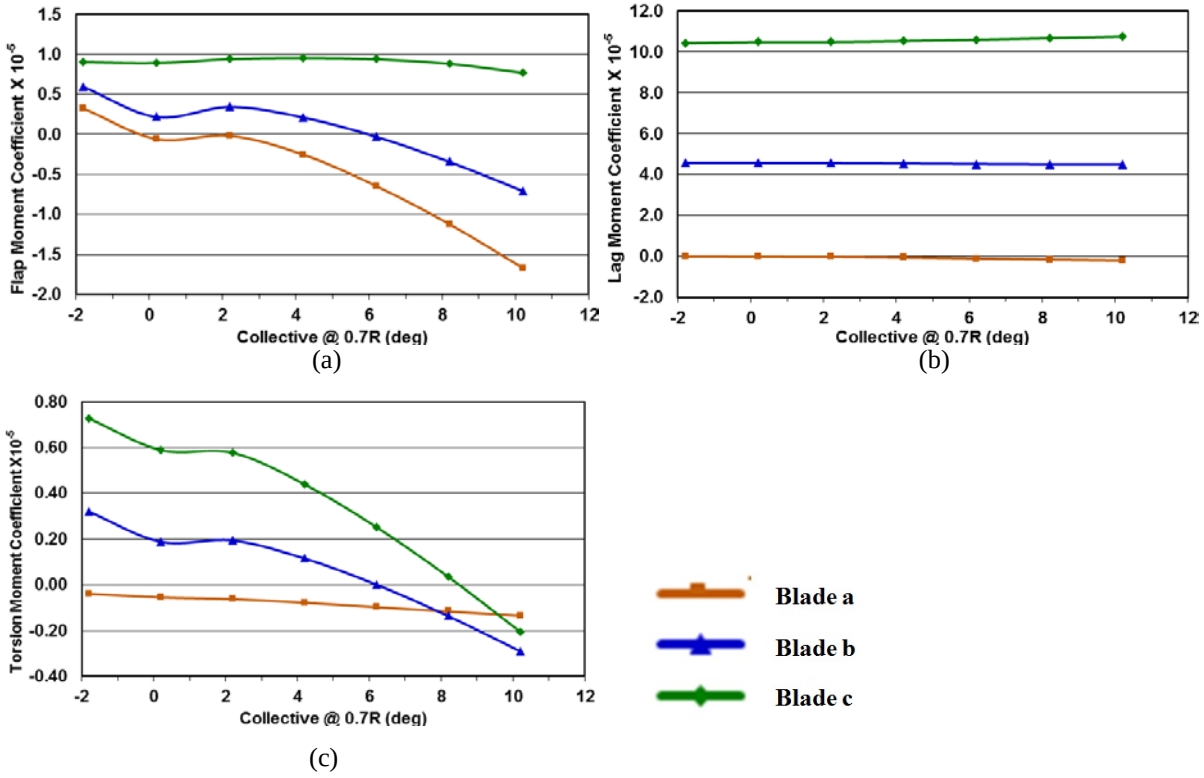

Figure 10: Double-sweep junction moments variations with variation in collective control

3.2.2 Cyclic input (along with collective)

Cyclic inputs produce oscillatory loads in the whirl tower blades. In this section, the effects of double-sweep on the blade oscillatory loads due to 2^o lateral cyclic, applied along with 5^o collective at 0.7R, are studied. The collective angle is given to avoid numerical convergence issues of the code by providing sufficient damping in flap bending. Figure 11 shows the root shear forces due to the combined cyclic and collective inputs. The flap shear forces are found to be less affected by introduction of double-sweep (Fig 11a). However, the oscillatory first harmonic component of the lag shear forces has slightly increased for blade *b* and blade *c* (Fig 11b).

Figure 12 shows the bending moments at the root. In the case of flap moments, the oscillatory components have reduced for blades *b* and *c* as compared to blade *a* (Fig 12a). However, the oscillatory components of lag and torsional moments have increased for blade *b* and blade *c*

as compared to blade *a* (Fig 12b). The cause of the higher harmonic content in the torsional moments is still under investigation.

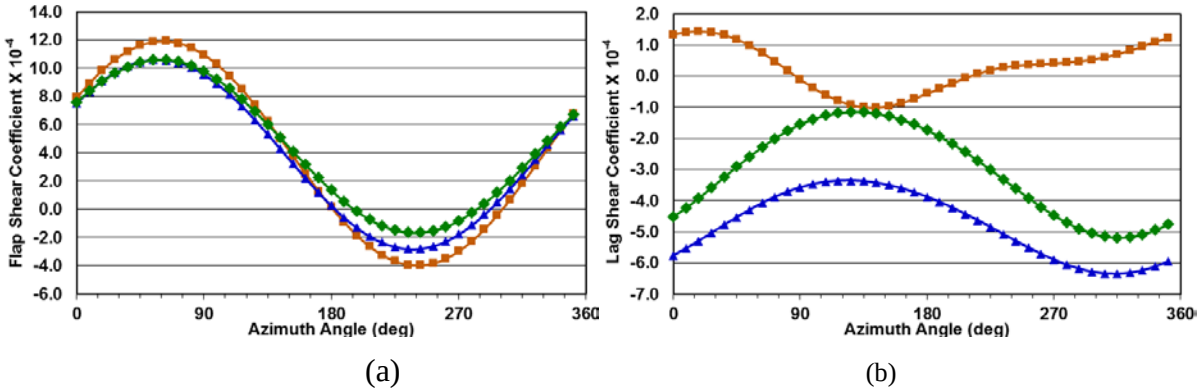

(a) (b)

Figure 11: Root shear forces variation with azimuth for combined cyclic and collective input

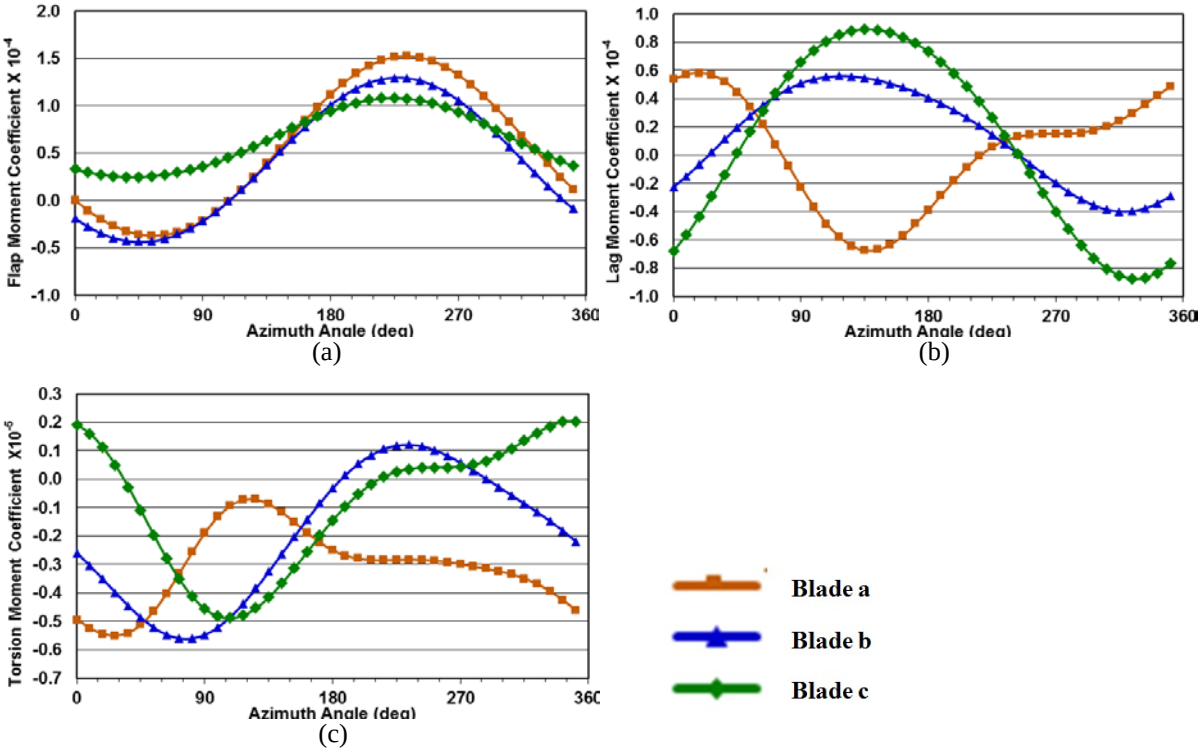

(a) (b) (c)

Figure 12: Root moments variations with azimuth for combined cyclic and collective input

Figure 13 shows the shear forces at the sweep junction. Both the flap shear forces (Fig 13a) and the lag shear forces (Fig 13b) at the sweep-junction follow the same trend as those at the root (Fig 11). Figure 14 shows the bending moments at the sweep junction. There is not much change in the oscillatory components of the flap (Fig 14a) and lag (Fig 14b) moments with introduction of double-sweep. However, the oscillatory component of the torsional moment has increased substantially for blades *b* and *c* as compared to blade *a*.

From the above analysis, it can be seen that the first harmonic oscillatory components of the flap shear force and flap moment are reduced with introduction of double-sweep. However, the first harmonic oscillatory components of the lag shear force, lag moment and torsional moments are, in general, increased.

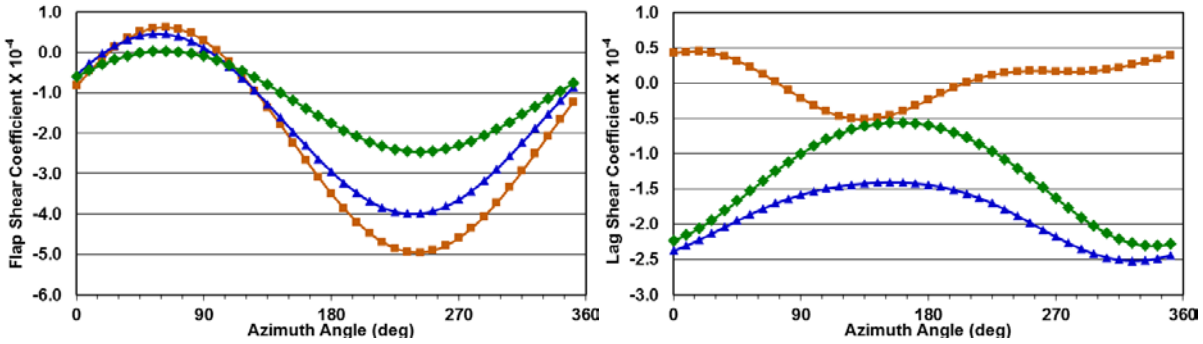

(a) (b)

Figure 13: Sweep-junction shear forces variation with azimuth for combined cyclic and collective input

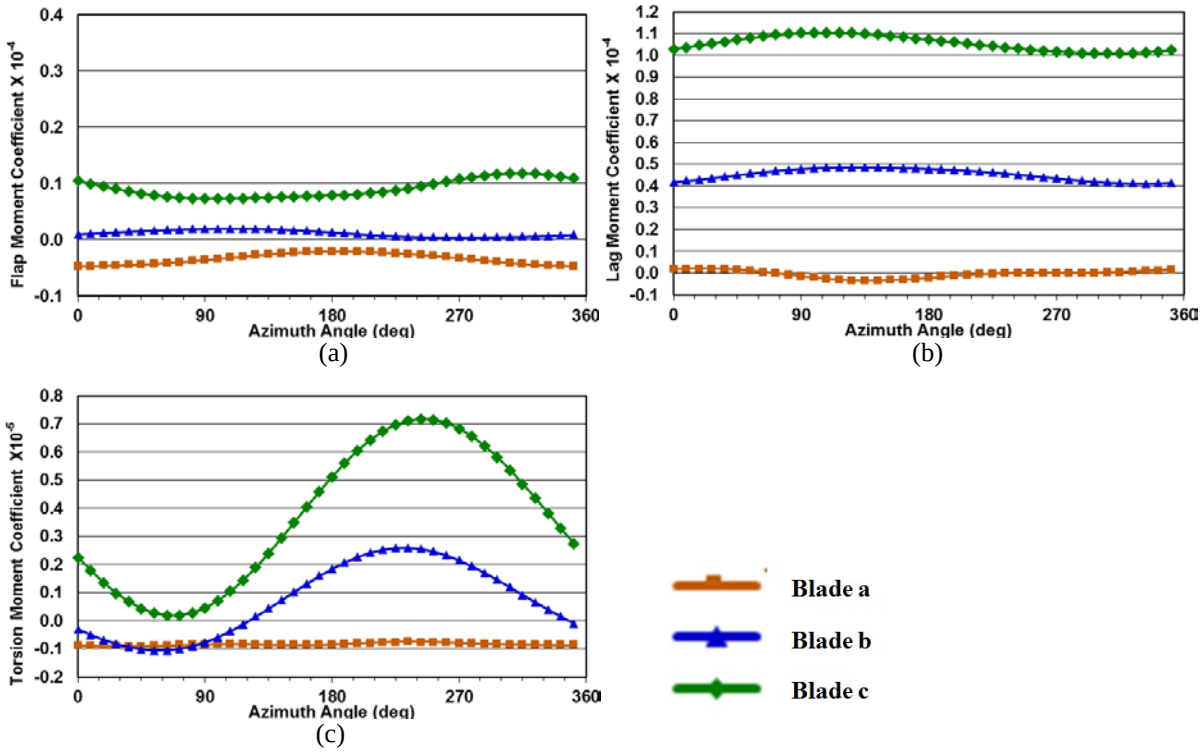

(a) (b)

(c)

Figure 14: Sweep-junction moments variations with azimuth for combined cyclic and collective input

4 CONCLUDING REMARKS

In this study, the dynamic characteristics of rotor blades with double-sweep and tip-anhedral were compared with those of a straight blade. Two blades were given the double-sweep features, one with mild sweep/anhedral angles and another with large sweep/anhedral angles. The following observations can be made based on this study:

1. The double-sweep with tip-anhedral geometry introduces bending-torsion-axial coupling in the rotor blade.
2. The natural frequencies of the rotor blade are dependent on the magnitude of the sweep/anhedral angles. The double-sweep causes a forward shift of all blade axes and therefore introduces an important flap-torsion coupling. This coupling affects the natural frequencies of the blade. 1st torsion and 3rd flap frequencies were seen to be the most affected.

3. In the whirl tower simulation with only collective input, it was seen that introduction of double-sweep led to slightly reduced power requirement. Minor changes were found for the flap shear forces and moments at the root however differences between the baseline and the swept blades for these loads were found to be slightly higher at the double-sweep junction. Major effects of the double-sweep were found for the lag shear forces at the root and the double-sweep junction for a collective control input. Here the double-sweep junction led to an increase in magnitude of the lag shear forces.
4. Whereas the torsional moment hardly was influenced by the collective control input for the baseline blade, a dependency of the torsional moment from the collective control input clearly could be seen for the swept blades with increased loads for low collective control inputs. By proper selection of the double-sweep shape parameters (angles), these loads can be minimized. Additional stiffening measures at the root may also be taken**.**
5. Similarly, in the whirl tower simulation with combined cyclic and collective inputs also, the double-sweep geometry resulted in reduction of the first harmonic oscillatory components of the flap shear force and flap moment. However, the first harmonic oscillatory components of the lag shear force, lag moment and torsional moments are, in general, increased**.**

5 REFERENCES

[1] Gervais, M., and V. Gareton, V., (2011). Analysis of Main Rotor Noise Reduction Due to Novel Planform Design – The Blue Edge™ Blade. *37th European Rotorcraft Forum*, Italy.

[2] Rauch, P., et al. (2011). Blue Edge™: The Design, Development and Testing of a New Blade Concept. *67th Annual Forum of the AHS*, USA.

[3] Truong, V. K., (2005). Dynamics studies of the ERATO blade, based on Finite Element Analysis. *31st European Rotorcraft Forum*, Italy.

[4] van der Wall, B. G., et al. (2016). From ERATO Basic Research to the Blue Edge™ Rotor Blade. *72nd Annual Forum of the AHS*, USA.

[5] Kumar, R., and Venkatesan, C. (2014). Rotorcraft aeroelastic analysis using dynamic wake/dynamic stall models and its validation. *Journal of Aeroelasticity and Structural Dynamics*, *3*(1).

[6] Kumar, M. R., and Venkatesan, C. (2016). Effects of blade configuration parameters on helicopter rotor structural dynamics and whirl tower loads. *The Aeronautical Journal* 120(1224), pp.271-290.

[7] Kumar, M.R. and Venkatesan, C. (2017). Effects of rotor blade-tip geometry on helicopter trim and control response. *The Aeronautical Journal*, pp.1-23. DOI: https://doi.org/10.1017/aer.2017.15

[8] Peters, D. A., and He, C. J. (1991). Correlation of Measured Induced Velocities with a Finite-State Wake Model. *Journal of the American Helicopter Society*, *36*(3), pp.59-70.

[9] Petot, D. (1989). Differential equation modeling of dynamic stall. *La Recherche Aerospatiale (English Edition)*, (5), pp.59-72

[10] McAlister, K. W., Lambert, O., and Petot, D. (1984). Application of the ONERA model of dynamic stall (No. NASA-A-9824). NASA, Moffett Field, CA, Ames Research Center.

[11] Rao, L. V., Kumar, M. R., and Venkatesan, C., (2015). Influence of Inflow States of Dynamic Wake Model on Trim, Rotor Loads and Control Response of Helicopter in Forward Flight. *41st European Rotorcraft Forum*, Germany.

[12] GSL – GNU Scientific Library, URL: http://www.gnu.org/software/gsl/

[13] Johnson, W. (1985). Recent developments in the dynamics of advanced rotor systems. NASA Technical Memorandum 86669.

COPYRIGHT STATEMENT